Journal of Ovarian Research

RESEARCH

Open Access

Mechanisms of He Shi Yu Lin formula in treating premature ovarian insufficiency: insights from network pharmacology and animal experiments

Yun Huang[1,2*], Qin Zhang[1], Dan Shen[1] and Xi Bao[1*]

Abstract

Objective He Shi Yu Lin Formula (HSYLF) is a clinically proven prescription for treating premature ovarian insufficiency (POI), and has shown a good curative effect. However, its molecular mechanisms are unclear. This study aimed to investigate the molecular mechanisms of HSYLF and clarify how network pharmacology analysis guides the design of animal experiments, including the selection of effective treatment doses and key targets, to ensure the relevance of the experimental results.

Methods Network pharmacology, molecular docking, and animal experiments were utilized to investigate the effects of HSYLF. Key targets were identified by intersecting herb and disease targets to construct protein–protein interaction and "active components-intersection targets-disease" networks. Gene Ontology and Kyoto Encyclopedia of Genes and Genomes pathway analyses were performed using the clusterProfiler package in R. A total of 50 specific pathogen-free female mice of reproductive age were included in the animal experiments. They were divided into five groups: the positive control group, the high-dose HSYLF group, the low-dose HSYLF group, the model blank group, and the normal control group, to evaluate the serum anti-müllerian hormone levels, mitochondrial morphology in oocytes, the levels of reactive oxygen species (ROS), and mitochondrial membrane potential.

Results Network pharmacology identified 204 active components connecting 219 key therapeutic targets for POI. Gene Ontology enrichment analysis indicated that the anti-POI targets of HSYLF mainly regulated response to xenobiotic stimulus, cellular response to chemical stress, and response to oxidative stress; and the Kyoto Encyclopedia of Genes and Genomes pathway analysis suggested the primary pathways, including lipid and atherosclerosis, advanced glycation end product-receptor for advanced glycation end product signaling pathway in diabetic complications, bladder cancer, tumor necrosis factor signaling pathway, and interleukin-17 signaling pathway. The low-dose (33 g/kg/d) HSYLF and high-dose (66 g/kg/d) HSYLF groups exhibited a marked elevation in serum anti-müllerian hormone levels (low-dose group: 2657.63 ± 354.82 PG/ml; high-dose group: 2823.73 ± 316.04 PG/ml) and mitochondrial membrane potential compared to the model blank group ($P < 0.05$ or $P < 0.01$), along with a significant decline in fluorescence intensity of 2′,7′-dichlorofluorescein for the levels of ROS in oocytes ($P < 0.05$ or $P < 0.01$). Additionally, both groups showed varying degrees of improvement in the morphology, quantity, and distribution of mitochondria.

*Correspondence:
Yun Huang
yhuang1871@sina.cn
Xi Bao
13735551911@163.com
Full list of author information is available at the end of the article

Conclusion This study provides definite evidence for the molecular mechanism by which HSYLF treats POI by decreasing mitochondrial ROS, increasing membrane potential, and improving mitochondrial function. The results from active components of HSYLF and their related key targets also confirmed the characteristics of its multi-component, multi-target, multi-pathway, and overall regulatory effects on POI. Further research regarding the mechanisms is required to generalize these results, and the deeper clinical value of HSYLF also needs to be investigated in the future.

Keywords Traditional Chinese medicine, Premature ovarian insufficiency, He Shi Yu Lin Formula, Network pharmacology, Mitochondria, Active oxygen

Introduction

Premature ovarian insufficiency (POI), a clinical syndrome, occurs in women under the age of 40. This disease is characterized by the loss of ovarian function leading to abnormal symptoms. Symptoms caused by low estrogen levels typically include infrequent menstruation, amenorrhea, hot flashes, night sweats, vaginal dryness, pain during sexual intercourse, arthralgia, urinary tract infection, anxiety, infertility, and cognitive dysfunction. These symptoms are accompanied by elevated levels of follicle-stimulating hormone and luteinizing hormone, along with low estrogen levels [1, 2]. Approximately 1% of women under 40 are affected by POI, with one of the most severe complications being reduced fertility rate. The chance of natural conception for patients is very low, typically between 4 and 5% [3]. The modern treatments for premature ovarian failure usually involve hormone replacement therapy, immunotherapy, ovulation induction, and ovarian tissue cryotransplantation. POI is primarily caused by kidney deficiency. From the perspective of traditional Chinese medicine (TCM) syndrome differentiation, the main therapeutic approaches involve tonifying and replenishing the kidneys, supplementing the qi, and nourishing the blood, which aligns with compatibility principles of He Shi Yu Lin Formula (HSYLF).

HSYLF was developed by He Jialin, a nationally renowned senior TCM practitioner. He inherited the expertise of the late elder chief physician He Zihuai of TCM, integrating decades of clinical experience and combining the theoretical and clinical essence of gynecology from two generations of the He's family. HSYLF consists of 14 Chinese herbal medicines, as listed in the Chinese Pharmacopoeia 2020 edition (Table 1) [4]. In a clinical study on HSYLF, 30 patients with diminished ovarian reserve function were divided by age into the low, middle, and high groups, each receiving oral HSYLF

Table 1 Herbal components of He Shi Yu Lin Formula

No	Chinese Name	Latin Name	Medicinal parts	Dosage in the study (g)
1	Bajitian	*Morinda officinalis F.C.How*	dried roots	10
2	Chuanxiong	*Ligusticum chuanxiong* Hort	dried roots	10
3	Danggui	*Angelica sinensis* (Oliv.) Diels	dried roots	10
4	Dangshen	*Codonopsis pilosula* (Franch.) Nannf., or *Codonopsis pilosula* Nannf. var. *modesta* (Nannf.) L. T. Shen, or *Codonopsis tangshen* Oliv	dried roots	15
5	Fangfeng	*Saposhnikovia divaricata* (Turcz.) Schischk	dried roots	5
6	Fupenzi	*Rubus chingii* Hu	dried fruits	15
7	Zhigancao	*Glycyrrhiza uralensis* Fisch., or *Glycyrrhiza inflata* Bat., or *Glycyrrhiza glabra* L	processed products of roots and rhizomes	3
8	Gouqizi	*Lycium barbarum* L	dried mature fruits	12
9	Roucongrong	*Cistanche deserticola* Y. C. Ma, or *Cistanche tuhulosa* (Schenk)	dried fleshy stems with scale leaves	10
10	Shechuangzi	*Cnidium monnieri* (L.) Cuss	dried mature fruits	6
11	Shudihuang	*Rehjnannia glutinosa* Libosch	processed products of root tubers	10
12	Tusizi	*Cuscuta australis* R. Br., or *Cuscuta chinensis* Lam	dried mature seeds	30
13	Xiangfu	*Cyperus rotundus* L	dried rhizoma	10
14	Yinyanghuo	*Epimedium brevicomu* Maxim., or *Epimedium sagittatum* (Sieb. et Zucc.) Maxim., or *Epimedium pubescens* Maxim., or *Epimedium koreanum* Nakai	dried leaves	15

treatment for three months. After treatment, the FSH levels are decreased across all age groups, and both fertility and ovarian reserve function are improved [4]. In an animal experiment using clomiphene as a control group, an investigation was conducted on the effect of HSYLF on model rats with kidney yang deficiency induced by intramuscular injection of hydrocortisone. The experimental results showed that HSYLF significantly increases the levels of serum estrogen and progesterone, enhances the expression intensity of estrogen receptors in the uterus and ovary, and improves the ultrastructure of the arcuate nucleus in the hypothalamus [5]. Another recent animal study found that HSYLF at low, medium, and high doses, administered by gavage, can increase the levels of anti-müllerian hormone (AMH) in mice with ovarian dysfunction, with the high-dose group exhibiting the most pronounced effect. The results of ovarian histology and follicle count suggested that HSYLF can promote the growth and development of follicles to a certain extent, thereby improving ovarian function [6].

Network pharmacology functions to systematically uncover the relevant mechanisms of multi-component drug therapy for diseases using bioinformatics and network analysis [7]. This network can demonstrate that a disease can be regulated by multiple genes, and conversely, a gene can regulate various diseases. Such results align with the theory of "different treatments for the same disease" and "same treatment for different diseases" in TCM. Additionally, network pharmacology can analyze the "multi-component and multi-target" action mechanisms of TCM from a holistic viewpoint, reflecting its "systematic and holistic" characteristics. This approach adheres to the TCM principles of "holistic view, syndrome differentiation, and treatment". By elucidating the molecular mechanism and material basis of TCM efficacy, network pharmacology can transform TCM research from empirical to evidence-based medicine. This is essential for the research and development of modern TCM, as it aims to delve deeper into the study of TCM formulas [8].

The purpose of this study was to explore the potential active components and targets of HSYLF in treating POI, as well as its molecular mechanism, providing relevant biological information support and animal experimental evidence for treating POI. The workflow is shown in Fig. 1.

Materials and methods

Collection and sorting of active components and related targets of HSYLF

Active components of HSYLF were screened from the Traditional Chinese Medicine Systems Pharmacology (TCMSP) database [9]. The components with clear targets were removed using oral bioavailability ≥ 30% and drug-likeness (DL) ≥ 0.18, and the related protein targets were merged and deduplicated.

Acquisition of POI-related targets

POI-related targets were identified using the keyword "POI" in the DsiGeNET and GeneCards databases [10]. These targets were then merged and deduplicated.

Screening of HSYLF targets against POI

To determine the potential targets of HSYLF against POI, the Venn Diagram package in R was used to analyze the common targets between HSYLF and POI.

Construction of PPI network

Based on the Search Tool for the Retrieval of Interacting Genes/Proteins database [11], HSYLF was identified as a potential therapeutic target for POI through protein–protein interaction (PPI) networks, with a confidence level of 0.9 and a species classification for *homo sapiens*. The PPI network and its topological characteristics were analyzed and visualized by Cytoscape 3.8.2 [12]. The degree of node genes was obtained and ranked, with the top five genes by PPI network degree selected as the hub genes.

Construction of the HSYLF-active components-hub gene network

The top five hub genes and the related active components of HSYLF for POI treatment were screened and imported into Cytoscape 3.8.2 to construct the pharmacological regulatory network of TCM.

GO function enrichment and KEGG pathway analysis

The clusterProfiler (v4.4.4) package in R was utilized to analyze the Gene Ontology (GO) biological function and the Kyoto Encyclopedia of Genes and Genomes (KEGG) signaling pathway enrichment of HSYLF and POI targets. Only data with a count > 1 and statistically significant differences (adjusted P) < 0.05 were retained in both GO and KEGG analyses.

Molecular docking

The three-dimensional structures of key target proteins were obtained from the Protein Data Bank database (http://www.rcsb.org/pdb) [13], with water molecules and other small molecules removed. Then, hydrogenation and charge calculations of the receptor were performed using the AutoDock (version 1.5.6) Tools [14]. The files for the related active components were downloaded from the PubChem database (https://pubchem.ncbi.nlm.nih.gov/) [15], and charge balance and rotatable bonds of ligands were checked by the AutoDock Tools.

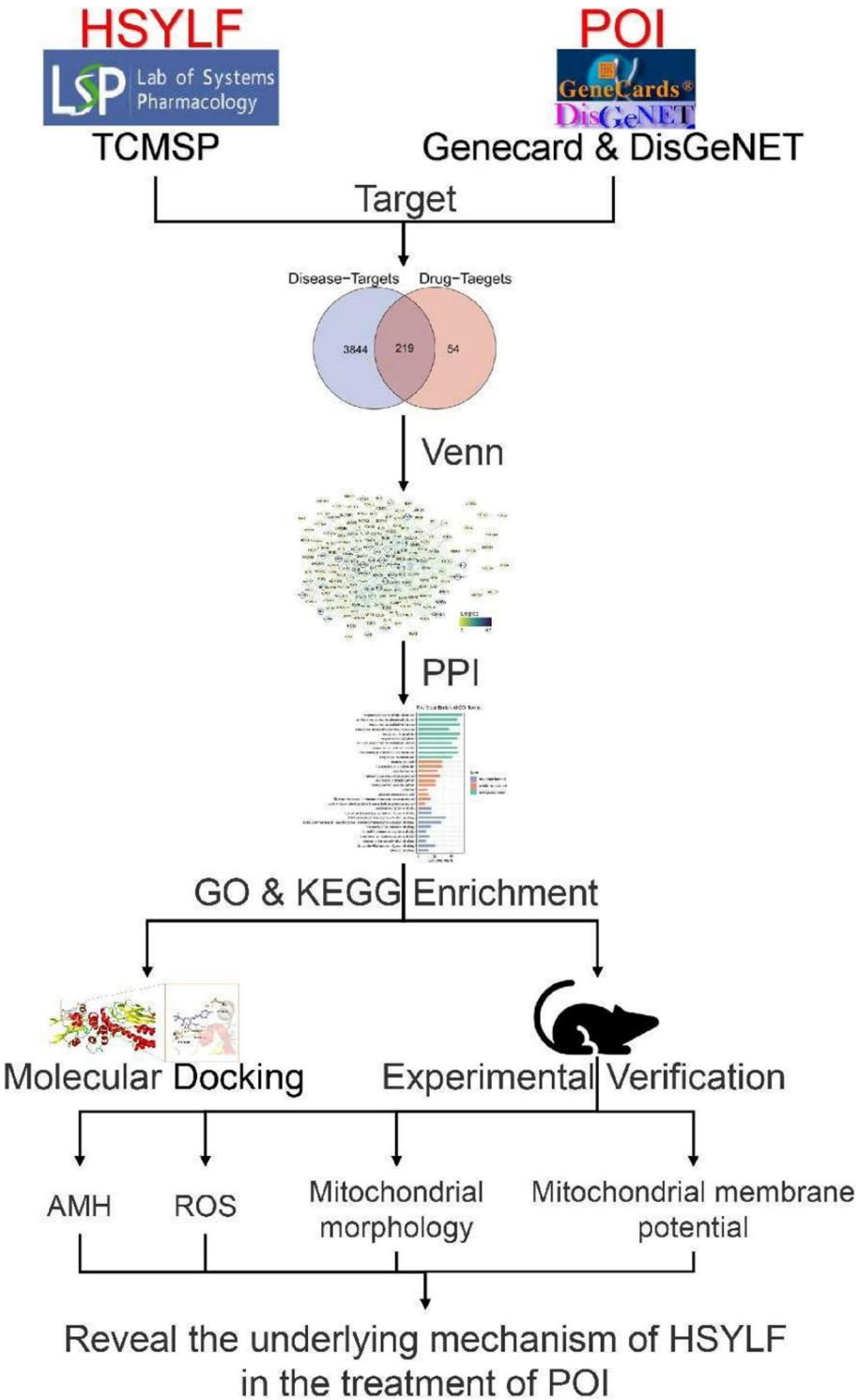

Fig. 1 The flow chart. HSYLF, He Shi Yu Lin Formula; POI, premature ovarian insufficiency; TCMSP, Traditional Chinese Medicine Systems Pharmacology; PPI, protein–protein interaction; GO, Gene Ontology; KEGG, Kyoto Encyclopedia of Genes and Genomes; AMH, anti-müllerian hormone; ROS, reactive oxygen species

Afterward, the dock boxes were selected according to the active center of the receptors. Lastly, molecular docking was conducted using the AutoDock Vina (version 1.1.2) to calculate the receptors as well as ligand docking [16]. To determine the optimal receptor-ligand complex, the poses with the lowest binding free energy affinity (such as the highest docking score) were selected as the visualization model through the PyMOL (version 2.5) software [17].

Medicines and reagents

HSYLF is a decoction composed of 14 Chinese herbal medicines, as listed in Table 1. These 14 herbs were purchased from Hangzhou Hospital of Traditional Chinese Medicine. The components of HSYLF were mixed in distilled water and soaked for 20 min (HSYLF:water: 1:10 mL/mL). Then, the mixture was heated to boiling, maintained for 10 min, and kept at a low heat for 1 h. After filtering out the aqueous phase, the filtrate and the mixture were combined and used for intragastric administration in experimental animals.

Other reagents used in the animal experiments are detailed in Supplementary Table S1.

Experimental setup and apparatus

The primary experimental setups and apparatuses are listed in Supplementary Table S2.

Animals

This study included 50 healthy, sexually mature female specific pathogen-free mice of reproductive age (6–8 weeks old), weighing 20–25 g. They were provided by the Shanghai SLAC Laboratory Animal Co. Ltd. (SCXK (Shanghai) 2022–0004). Mice at 6–8 weeks of age were selected because, at this stage, their reproductive systems are fully developed and their health index is high, effectively minimizing the impact of their own health status or any decline in reproductive function on the experimental results.

Each mouse was maintained under controlled environmental conditions ((25 ± 3 °C), humidity (50 ± 5%), and 12-h light/dark cycle). The mice were provided with nutritionally complete pellet feed and reverse osmosis water.

The animal study protocol was approved by the Animal Ethics Committee of Zhejiang Chinese Medical University for the handling of animals (protocol approval number: 20220639), and researchers involved in this study received training in the care and handling of laboratory animals.

Design of pharmacodynamics animal experiment

At 9:00 AM, vaginal smears were collected from the mice and examined cytologically under an optical microscope. To confirm the normal estrous cycle, the exfoliated vaginal cell smears of these female mice were observed for 6 consecutive days [18, 19]. Then, the 50 mice with a normal estrous cycle were selected and randomly divided into the normal control group ($n = 10$), and the pre-modeling group ($n = 40$). Except for the normal control group, all other groups underwent modeling: on day 1, the 40 mice received an intraperitoneal injection of cyclophosphamide (50 mg/kg) diluted in normal saline (1 mL), followed by daily intraperitoneal injections of cyclophosphamide (10 mg/kg) diluted in normal saline (1 mL) from days 2 to 14 [20, 21]. The estrous cycle of the mice was monitored, with disruptions or prolonged intervals indicating successful modeling. After modeling, the 40 mice were randomly allocated into the following four groups ($n = 10$): the positive control group, the high-dose HSYLF group, the low-dose HSYLF group, and the model blank group. The positive control group was given 0.3 mL of coenzyme Q10 solution, while the normal control and model blank control groups received distilled water. Based on the "table of equivalent dose proportion of human and animal body surfaces ". The mice in the low-dose HSYLF and high-dose HSYLF groups were treated with 33 g/kg and 66 g/kg of TCM once a day, respectively. All drugs were administered once daily at 9:00 a.m. for 6 weeks.

Preparation of mouse samples

After 6 weeks of administration, each female mouse underwent superovulation via an intraperitoneal injection of 10 IU of pregnant mare serum gonadotropin and 10 IU of human chorionic gonadotropin after 48 h. Then, 14–16 h later, the blood from the orbit was extracted and centrifuged to obtain serum. The mice were euthanized by by CO_2 asphyxiation, and the abdominal wall was opened to expose the bilateral ovaries. The ovaries were carefully dissected, and the follicles were punctured to release cumulus-oocyte complexes (COCs). The COCs were cultured in the medium for 17 h. During this process, cumulus cells were separated from the oocytes, and the denuded oocytes (DOs) were collected and stored in sterile tubes.

Observation indices and detection methods

The effects of HSYLF on AMH levels, mitochondrial function, and oxidative stress were assessed based on the aforementioned analysis of network pharmacology.

Serum AMH levels in mice were determined. Mouse blood samples were left to stand and centrifuged at

3000 rpm for 20 min. Then, the supernatant was collected and stored at -20℃. Serum AMH levels were measured using the enzyme-Linked Immunosorbent Assay Kit according to the manufacturer's instructions.

Mitochondrial morphology of oocytes was measured. The ovaries were sectioned into 1 mm × 1 mm × 1 mm tissue blocks and fixed in 3% glutaraldehyde at 4 ℃ for 24 h. Next, the fixative was washed off, and the tissue was fixed with 1% osmium tetroxide for 90 min. Following dehydration, embedding, and trimming, ultrathin sections were obtained using an ultramicrotomy. The sections were stained with 4% uranyl acetate and lead citrate. After naturally drying, the sections were examined by the scanning electron microscopy.

Determination of ROS in oocytes was conducted. The cell suspension was prepared from cells in the logarithmic growth phase. Upon adding 2′,7′-dichlorofluorescein diacetate, the cell suspension was incubated for 20 min, followed by three washes with serum-free cell culture solution. Subsequently, the cells were in 4% paraformaldehyde for 10 min and washed three times with phosphate-buffered saline. The suspension was also stained with 4′,6-diamidino-2-phenylindole, and incubated for 2 min at room temperature in the dark. After that, the suspension was rinsed three times with phosphate-buffered saline, each for 5 min. Sealed sections were observed and photographed under an inverted fluorescence microscope.

Measurement of mitochondrial membrane potential was performed. The stock solution of JC-1 was dissolved in dimethyl sulfoxide, with the final concentration of dimethyl sulfoxide used set to 25 mmol/L. The solution was aliquoted and stored at -20%. The solution was allowed to at room temperature for 1 h until use. The oocytes were transferred into the transfection solution and incubated in the dark for 15 min. Afterward, the oocytes were subjected to three washes in an M16 medium and observed using the confocal microscope. Red fluorescence was measured at an excitation wavelength of 559 nm and an emission wavelength of 572 nm, while green fluorescence was detected at 488 nm excitation and 520 nm emission. Measurements of fluorescence intensity were carried out, and red-to-green fluorescence intensity ratio was used to calculate the mitochondrial membrane potential.

Statistical analysis

Data analysis was performed using SPSS 16.0. Results were expressed as mean ± standard deviation. The t-test was used for comparisons between two groups, and one-way analysis of variance was employed to compare the data among multiple groups. If data met normal distribution and homogeneity of variance, pairwise comparisons were further analyzed using the Tukey's test. For the normal distribution with unequal variances, the Dunnett's T3 test or independent t-test was applied. For the non-normal distribution, the Kruskal–Wallis H test was adopted. $P < 0.05$ was considered statistically significant.

Results

Collection and classification of active components and related targets in HSYLF

Using the TCMSP database, 14 Chinese herbal medicines of HSYLF were retrieved, and the active components identified included 174 components from Bajitian, 189 from Chuanxiong, 125 from Danggui, 134 from Dangshen, 173 from Fangfeng, 110 from Fupenzi, 280 from Zhigancao, 188 from Gouqizi, 75 from Roucongrong, 114 from Shechuangzi, 76 from Shudihuang, 29 from Tusizi, 104 from Xiangfu, and 130 from Yinyanghuo. The active components of drugs were screened according to oral bioavailability > 30% and drug-likeness > 0.18, identifying 204 active components. Detailed information on these potential active compounds in HSYLF is displayed in Supplementary Table S3. A total of 273 related targets were obtained for subsequent analysis based on the active components of each herb.

Acquisition of POI-related targets

The GeneCards database provided 3,996 POI-related targets, while 299 POI-related disease targets were retrieved from the DisGeNET. After merging and deduplication of the two datasets, a total of 4,063 POI-related targets were obtained.

Screening of targets of HSYLF against POI

The intersection of the above-obtained drug targets and POI disease targets was calculated using the Venn package in R (version 1.11), resulting in 219 key targets (Fig. 2).

Construction of PPI network

The PPI networks were constructed for the 219 targets with a confidence level of 0.9. A total of 189 proteins and 930 edges were identified. After that, Cytoscape software was used to refine the protein network diagram, as shown in Figure S1. The topological characteristics of the PPI network were analyzed to obtain the degree of node genes. The top five genes were ranked and obtained: tumor protein p53 (TP53), jun proto-oncogene (JUN), mitogen-activated protein kinase (MAPK) 3, heat shock protein 90 alpha family class A member 1, and signal transduction and activator of transcription (STAT) 3. These top genes were designated as hub genes (Table S4).

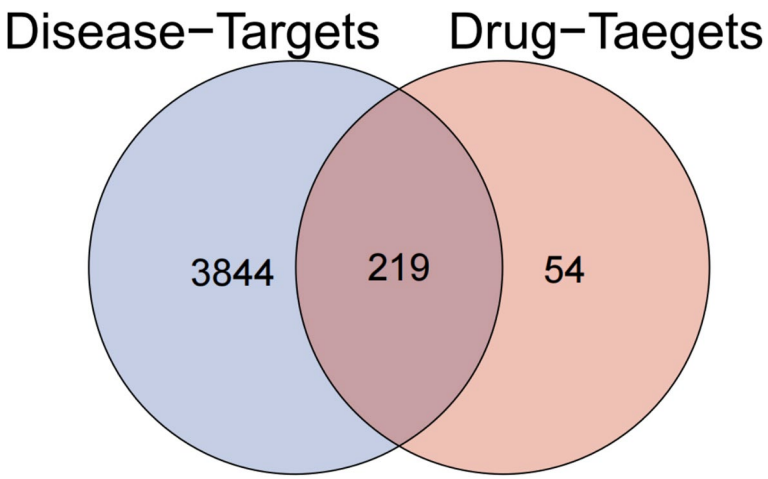

Fig. 2 Venn diagram of intersection in HSYLF targets and POI targets

Construction of the HSYLF-active components-hub gene network

Based on the five hub genes mentioned above, their related components were selected, and the disease-active components-hub gene network was constructed and visualized using the Cytoscape software. The network contained 13 herbs, 102 active components, five key targets, and 243 relationship pairs (Fig. 3).

GO function enrichment and KEGG pathway analysis

Through the GO function enrichment analysis using R language software, 2,454 terms were identified in biological processes (BP), such as response to xenobiotic stimulus, cellular response to chemical stress, response to oxidative stress, response to reactive oxygen species (ROS), response to peptide, response to radiation, response to nutrient levels, response to extracellular stimulus, and response to metal ions, all of which were significantly correlated in BP. In cellular components (CF), a total of 185 terms were obtained, including membrane raft, membrane microdomain, vesicle lumen, transcription regulator complex, secretory granule lumen, cytoplasmic vesicle lumen, caveola, plasma membrane raft, RNA polymerase ll transcription regulator complex, and cyclin-dependent protein kinase holoenzyme complex. These were the comparatively significant correlated functions. In molecular functions (MF), 101 terms were identified, with significant components such as nuclear receptor activity, ligand-activated transcription factor activity, DNA-binding transcription factor binding, RNA polymerase ll-specific DNA-binding transcription factor binding, transcription cofactor binding, steroid hormone receptor activity, neurotransmitter receptor activity, transcription coactivator binding, ubiquitin-like protein ligase binding, and steroid binding (Fig. 4).

KEGG pathway enrichment analysis identified 164 enrichment pathways, with the top 20 pathways illustrated in Fig. 5. The significant pathways related to disease included lipid and atherosclerosis, advanced glycation end product (AGE)-receptor for AGE (RAGE) signaling pathway in diabetic complications, hepatitis B, chemical carcinogenesis—receptor activation, prostate cancer, fluid shear stress and atherosclerosis, pancreatic cancer, interleukin-17 signaling pathway, bladder cancer, hepatitis C, tumor necrosis factor (TNF) signaling pathway, non-small cell lung cancer, Kaposi sarcoma-associated herpesvirus infection, small cell lung cancer, endocrine resistance, toxoplasmosis, measles, human cytomegalovirus infection, Epstein-Barr virus infection, and colorectal cancer.

Key target function/pathway regulatory network diagram

The top 20 targets corresponding to GO-CC, GO-BP, and GO-MF were identified, and the compounds targeting them were isolated. A regulatory network diagram of key target functions was constructed and visualized through Cytoscape software, as shown in Figure S2. In the BP key target network, there were 10 BP entries, 131 key targets, and 460 interaction pairs. In the CC key target network, 10 MF entries, 79 key targets, and 195 interaction pairs were identified. The key target MF network contained 10 CC entries, 70 key targets, and 171 interaction pairs.

A list of the top 20 KEGG pathways and their corresponding key targets was compiled, alongside the compounds specific to each key target. The regulatory network diagram of key target pathways was using Cytoscape software, as displayed in Figure S3. The

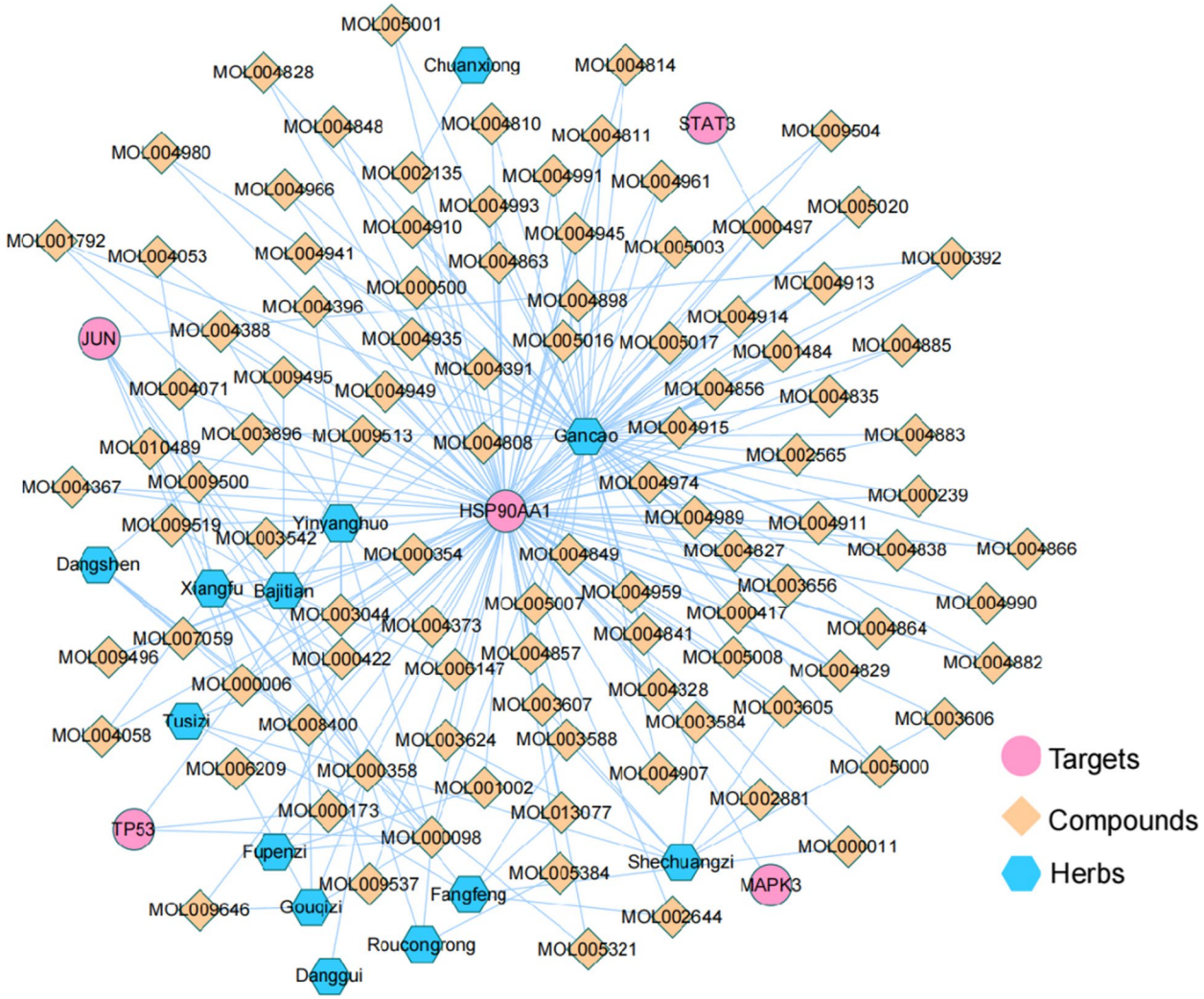

Fig. 3 Pharmacological regulatory network of TCM on key targets

network contained 20 KEGG pathways, 119 key targets, and a total of 607 interaction pairs.

Molecular docking

The related active molecules for hub genes were identified in the TCM pharmacology network, and the herbs with active components were prioritized in the TCMSP database. The receptors and ligands in docking are shown in Table 2. The visualization mode of docking results is presented in Fig. 6.

Serum AMH levels of mice

Serum AMH levels in the model blank group were significantly lower compared to the normal control group ($P < 0.01$, Fig. 7). In contrast, there was a marked elevation in the serum AMH levels in the positive control, low-dose HSYLF, and high-dose HSYLF groups as opposed to the model blank group ($P < 0.05$ or $P < 0.01$). These findings indicated that HSYLF improved ovarian function in mice, supporting the hypothesis that it might enhance ovarian function and delay insufficiency by increasing the AMH levels.

Mitochondrial morphology in oocytes

The electron microscope revealed numerous mitochondria in the normal control group, with normal morphology, basically round shape, moderate distribution density, and a clear and distinct inner ridge (Fig. 8). Compared with the normal control group, the model blank group showed enlarged average mitochondrial volume, and reduced specific surface area, density and numbers, along with signs of white vacuole-like changes, swelling of the Golgi apparatus, and endoplasmic reticulum. Improvements in mitochondrial morphology, quantity,

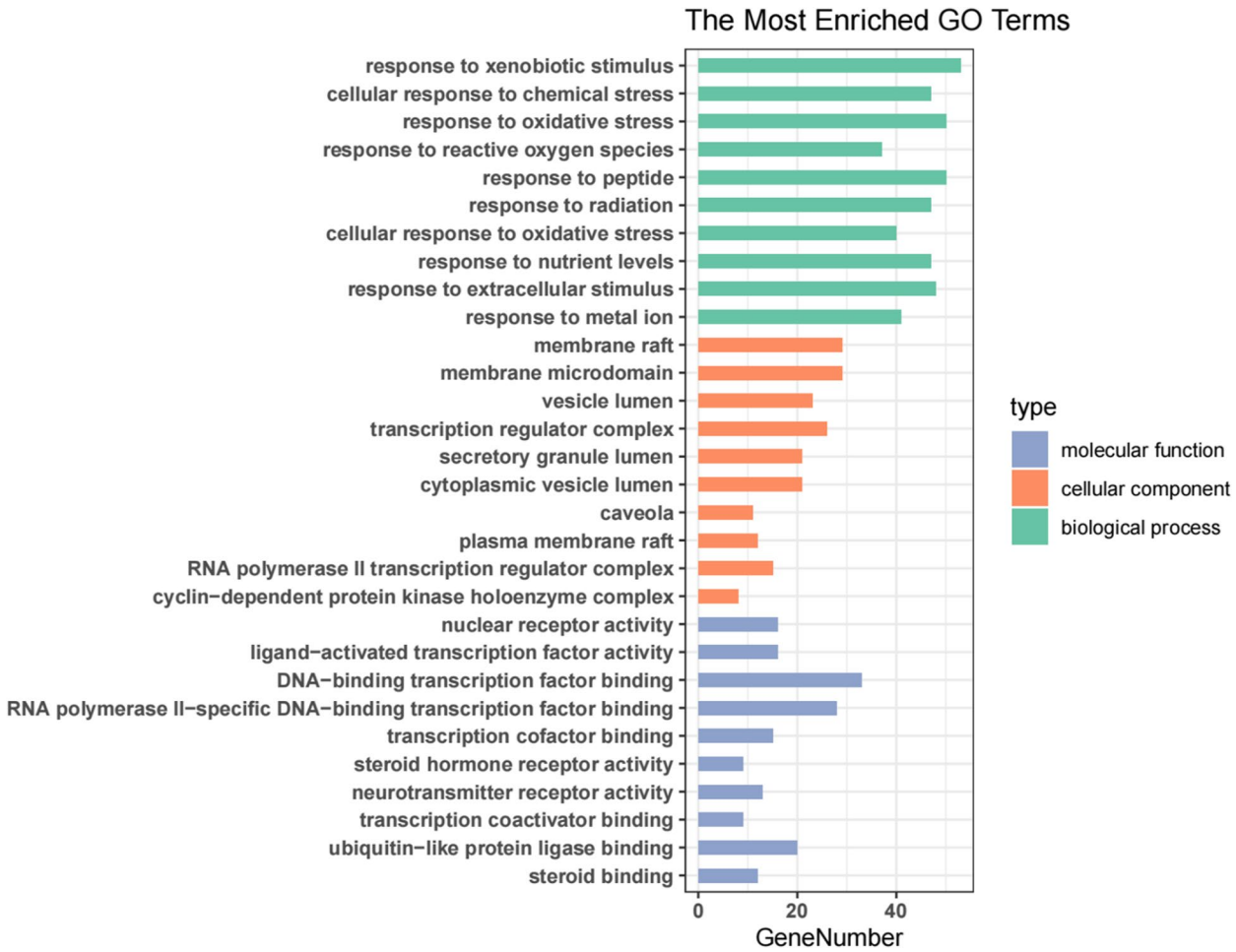

Fig. 4 Bar chart for top 10 GO enrichment

and distribution were observed in the positive control, low-dose HSYLF, and high-dose HSYLF groups to varying extents. These results revealed that HSYLF treatment improved mitochondrial morphology, quantity, and distribution in the ovarian tissues of model mice, suggesting its potential therapeutic effect on POI through the regulation of mitochondrial function.

Determination of ROS in oocytes

According to Figs. 9A–B, the fluorescence intensity of 2′,7′-dichlorofluorescein was significantly higher in oocytes of mice in the model blank group than that in the normal control group ($P<0.01$). In contrast to the model blank group, there was a remarkable reduction in the fluorescence intensity of 2′,7′-dichlorofluorescein in oocytes in the positive control, low-dose HSYLF, and high-dose HSYLF groups ($P<0.05$ or $P<0.01$). Therefore, HSYLF treatment significantly reduces the ROS levels in the oocytes of model mice, indicating its potential protective effect on ovarian function by alleviating oxidative stress and supporting its potential intervention in POI.

Determination of mitochondrial membrane potential

As shown in Fig. 10, the mitochondrial membrane potential of oocytes was significantly decreased in the model blank group compared with the normal control group ($P<0.01$). Additionally, the mitochondrial membrane potential was notably elevated in the positive control, low-dose HSYLF, and high-dose HSYLF groups relative to the model blank group ($P<0.05$ or $P<0.01$). According to Fig. 10A, changes in aggregate (red) and monomer (green) fluorescence in the HSYLF treatment groups indicated a restorative effect of HSYLF on mitochondrial membrane potential. The fluorescence quantification results further demonstrated the degree of improvement in mitochondrial function (Fig. 10B). These results supported the hypothesis that HSYLF might improve ovarian function by enhancing mitochondrial function.

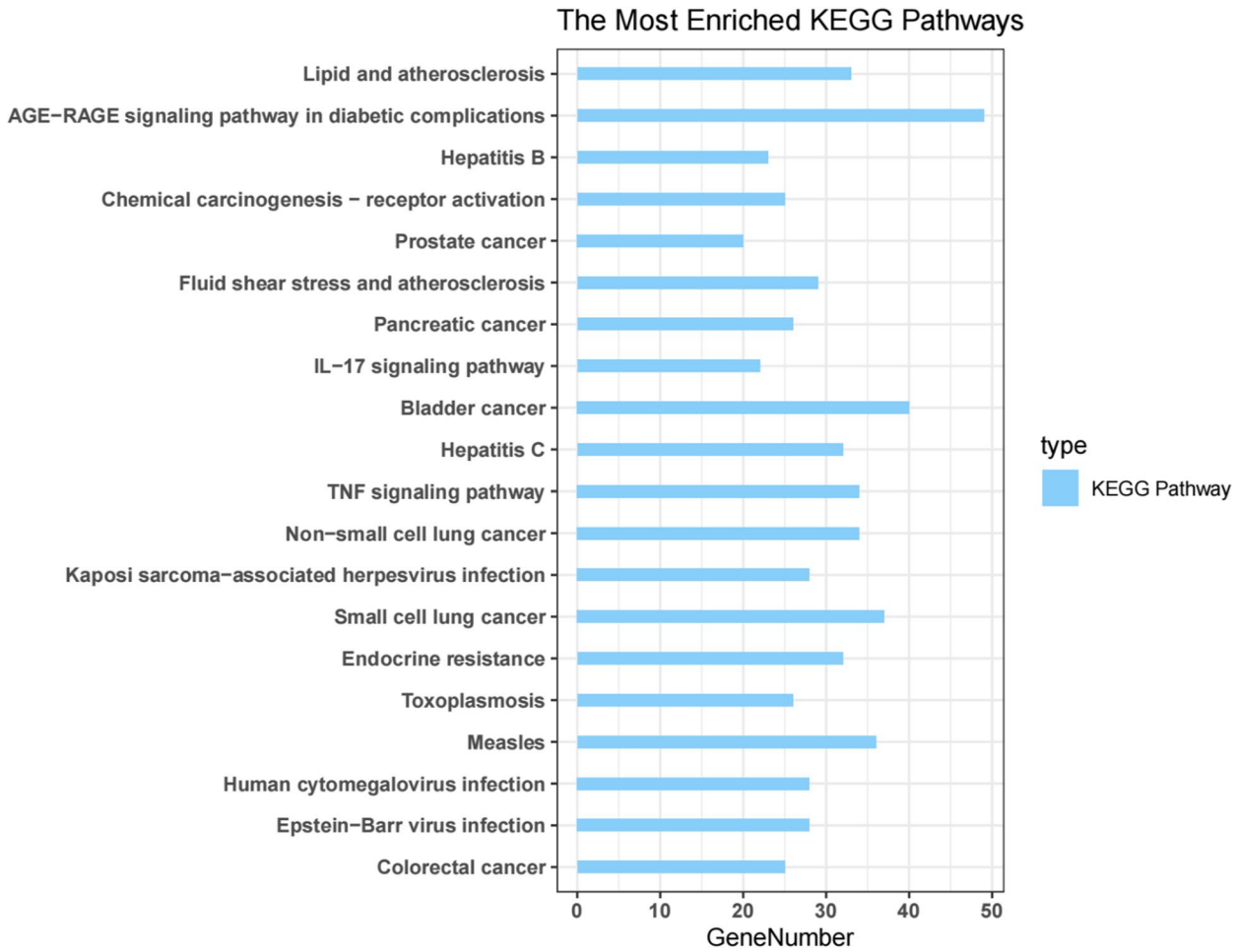

Fig. 5 Bar chart of the top 20 KEGG pathways for HSYLF targets in POI treatment, highlighting lipid metabolism, AGE-RAGE signaling, and cancer-related pathways. KEGG, Kyoto Encyclopedia of Genes and Genomes; HSYLF, He Shi Yu Lin Formula; POI, premature ovarian insufficiency; AGE-RAGE, advanced glycation end product-receptor for advanced glycation end product

Table 2 Receptors and ligands in docking

MOL_ID	PDB ID	molecule_name	OB	MW	DL	Targets	Score kcal/mol
MOL009500	1byq	1,6-dihydroxy-5-methoxy-2-(methoxymethyl)-9,10-anthraquinone	104.54	314.31	0.34	HSP90AA1	-7.5
MOL000392	1jnm	formononetin	69.68	268.28	0.21	JUN	-7.1
MOL004328	2zoq	naringenin	59.29	272.27	0.21	MAPK3	-8.7
MOL000497	6njs	licochalcone A	40.79	338.43	0.28	STAT3	-6.6
MOL000098	1aie	quercetin	46.43	302.25	0.28	TP53	-6.5

PDB Protein Data Bank, *OB* oral bioavailability, *MW* molecular weight, *DL* drug-likeness, *JUN* jun proto-oncogene, *MAPK3* mitogen-activated protein kinase 3, *HSP90AA1* heat shock protein 90 alpha family class A member 1, *STAT3* signal transduction and activator of transcription, *TP53* tumor protein P53

Discussion

POI refers to the cessation of ovarian function before the age of 40. According to a recently published meta-analysis, the global prevalence of this disease is estimated at 3.7% [22]. Currently, treating POI with recognized and reliable methods remains challenging. In this field, Chinese herbal medicines, such as HSYLF, are gaining increasing popularity.

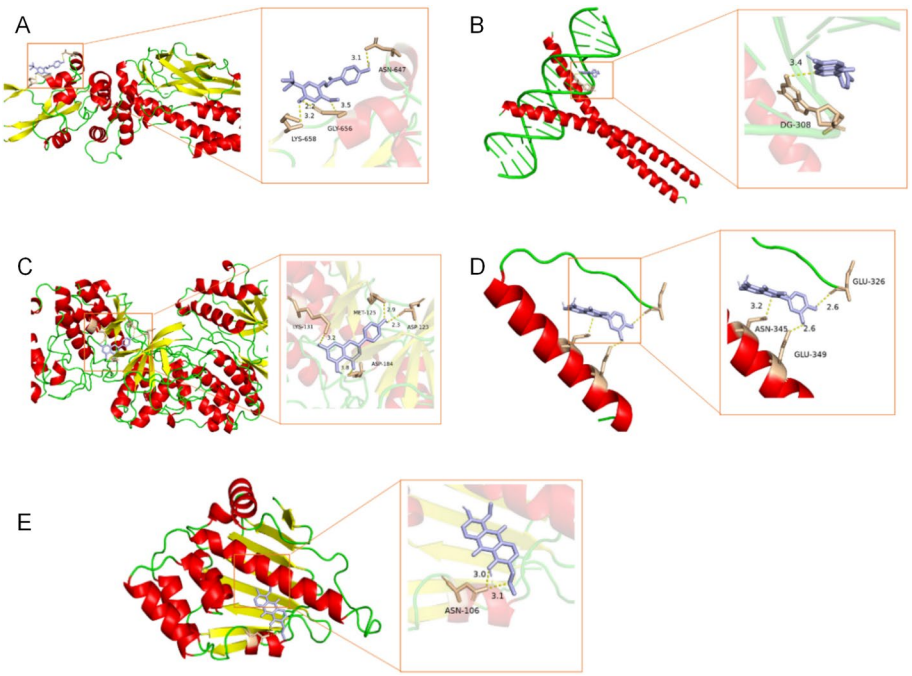

Fig. 6 Molecular docking results of HSYLF with high binding energy. **A** STAT3 and licochalcone A; **B** Jun and formononetin; **C** MAPK3 and naringenin; **D** TP53 and quercetin; **E** HSP90AA1 and 1,6-dihydroxy-5-methoxy-2-(methoxymethyl)-9,10-anthraquinone. HSYLF, He Shi Yu Lin Formula; STAT3, signal transduction and activator of transcription; Jun, Jun proto-oncogene; MAPK3: mitogen-activated protein kinase 3; TP53, tumor protein P53; HSP90AA1, heat shock protein 90 alpha family class A member 1

The mechanism of Yulin Formula in treating cyclophosphamide-induced diminished ovarian reserve has been reported. This mechanism highlights that YLF significantly reduces ovarian cell apoptosis and improves ovarian function by regulating the phosphatidylinositol 3-kinase/AKT signaling pathway, leading to an increase in AMH levels close to normal. Such a result provides theoretical support for the application of YLF in the field of reproductive health [23]. In this study, special attention is given to investigating the effects of HSYLF on POI. To better understand the mechanisms of HSYLF in treating POI, mice were used as animal models in pharmacodynamic experiments, and network pharmacology and molecular docking techniques were employed to investigate the chemical components and targets of HSYLF. Through network pharmacology analysis, 204 active components and 219 key genes identified in HSYLF were associated with POI. Herbs in HSYLF with higher active components included formononetin, naringenin, licochalcone A, and quercetin. Among them, formononetin, a phytoestrogen, can bind to estrogen receptors due to its structural similarity to estrogen [24]. As an estrogen-like compound, formononetin can enhance estrogen-like functions by increasing the expression of estrogen receptor proteins [25]. Additionally, formononetin can reduce the ROS levels by activating the phosphatidylinositol 3-kinase/AKT and nuclear factor erythroid 2-related factor 2 signal pathways and increasing the antioxidant gene expression [26]. Naringenin exhibits good corrosion inhibition performance and acts as a chemical group and a scavenger (superoxide dismutase). Additionally,

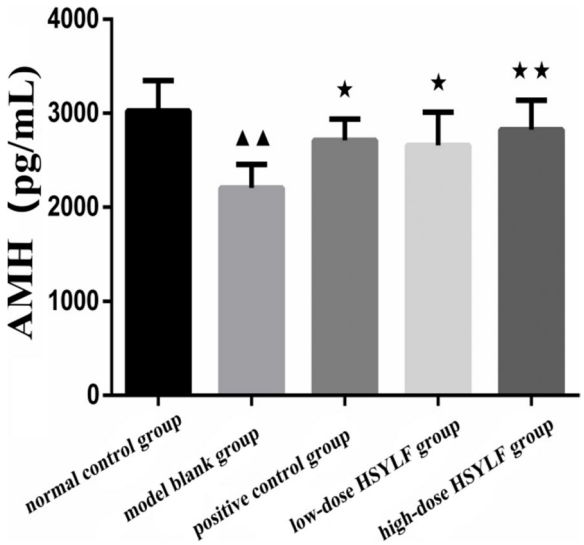

Fig. 7 HSYLF treatment increases serum AMH levels in mice with POI. ▲▲$P<0.01$, ★$P<0.05$, and ★★$P<0.01$ *vs.* normal control group ($n=8$)

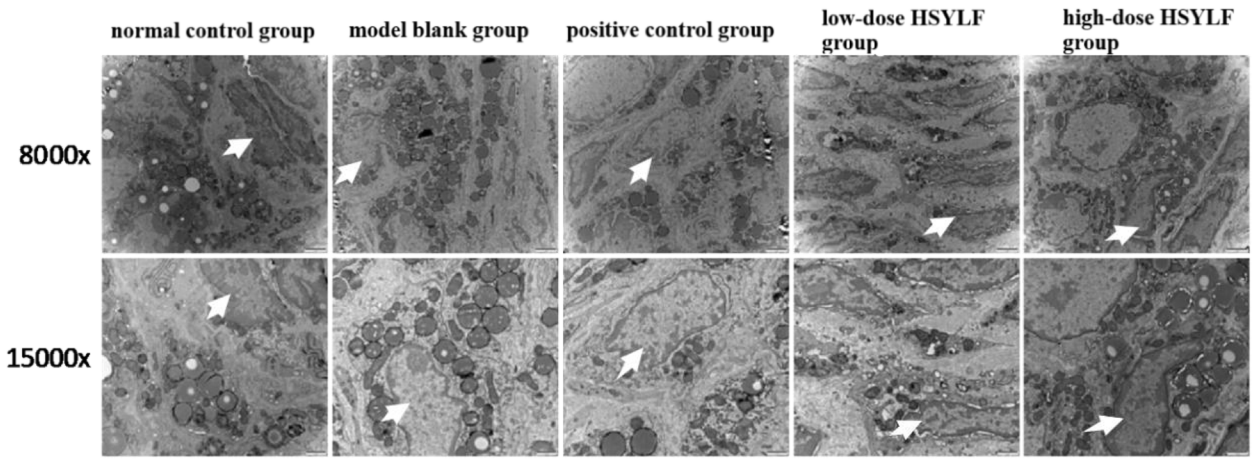

Fig. 8 HSYLF treatment improves the morphology and function of mitochondria in ovarian tissue of mice with POI. Magnification and scale bar (8000×, 2 μm; 15,000×, 1 μm), with white arrows marking the mitochondria

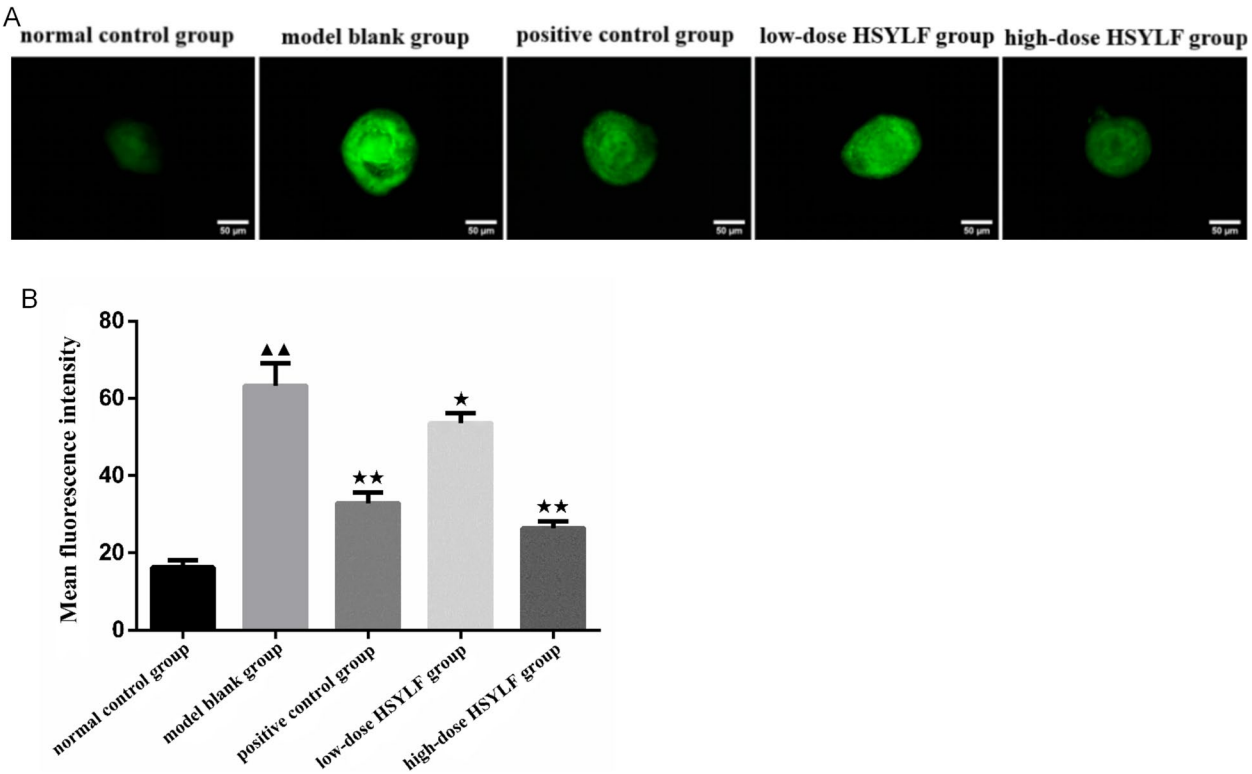

Fig. 9 HSYLF significantly reduces ROS levels in oocytes of mice with POI to protect ovarian function. **A**–**B** DCF fluorescence images and the expression in oocytes of mice in different groups. Magnification and scale bar: (400×, 50 μm). ▲▲$P < 0.01$ *vs*. normal control group; ★$P < 0.05$, ★★$P < 0.01$ *vs*. model blank group ($n = 3$). ROS, reactive oxygen species; DCF, 2′,7′-dichlorofluorescein; POI, premature ovarian insufficiency

it functions as a free radical scavenger and inhibits the activities of oxygen promoting enzymes, such as nicotinamide, adenine dinucleotide phosphate oxidase, cyclooxygenase, lipoxygenase, xanthine oxidase, and metal ion chelation [27]. Consequently, naringenin can inhibit inflammatory responses, protect mitochondrial function, and inhibit apoptosis [28–31]. Moreover, due to the antioxidant properties of quercetin, it can reduce DNA

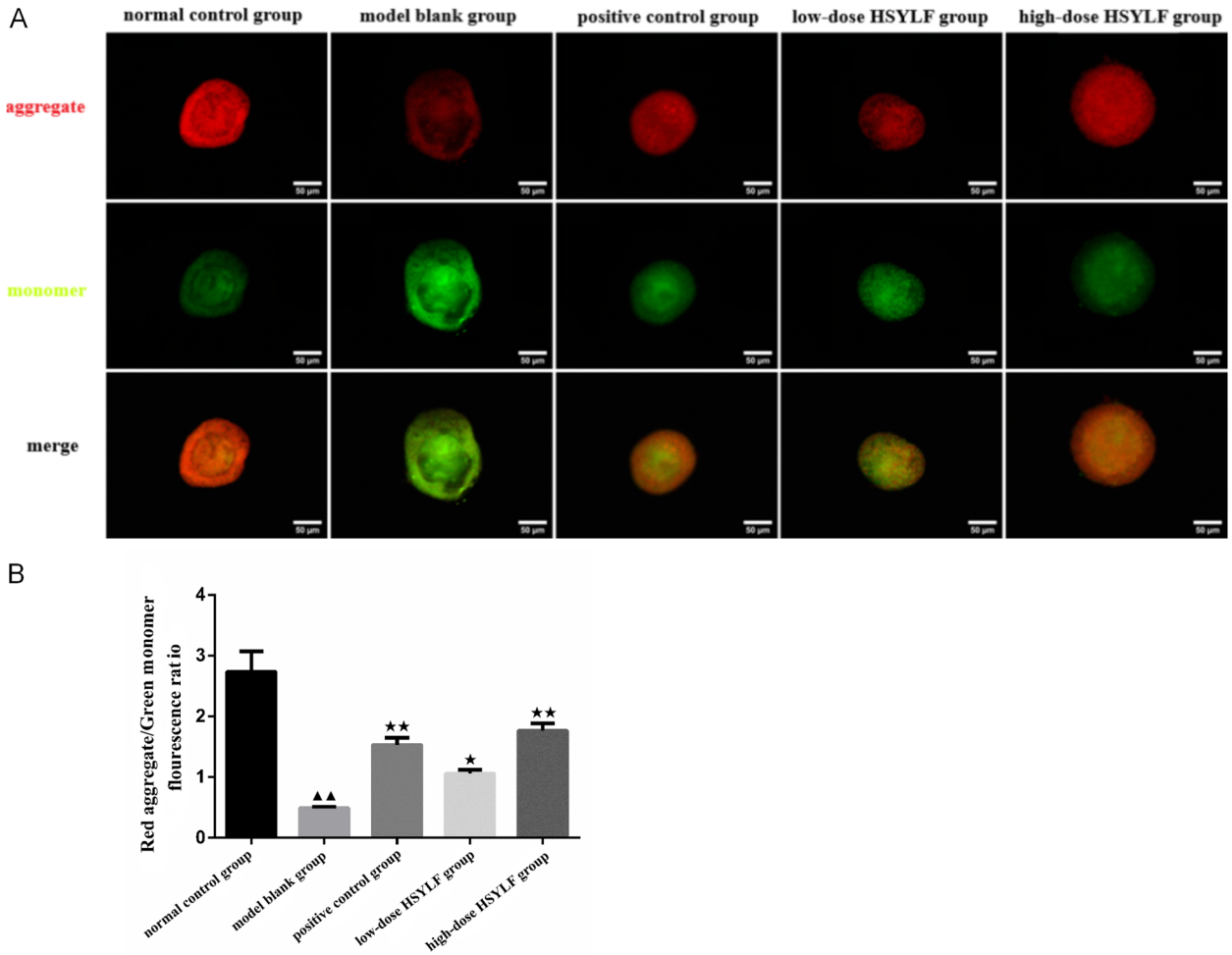

Fig. 10 HSYLF treatment enhances mitochondrial membrane potential in oocytes of mice with POI. **A** Changes in the mitochondrial membrane potential of mice in oocytes in different groups. Magnification and scale bar: (400×, 50 μm); **B** Fluorescence quantification results of mice in oocytes in different groups. ▲▲$P < 0.01$ *vs*. normal control group; ★$P < 0.05$, ★★$P < 0.01$ *vs*. model blank group ($n = 3$)

damage, mitochondrial damage, endoplasmic reticulum damage, and cellular damage caused by reactive oxygen free radicals [32]. The molecular docking results indicated that these active components have potential binding affinities with therapeutic targets for POI, indicating a moderate potential for binding. Hydrogen bonding interactions were observed between residues Asn-647, Lys-658, and Gly-656 with licochalcone A molecules; residue DG-308 with formononetin molecules; residues ASP-184, LYS-131, MET-125, and ASP-123 with naringenin molecules; residue ASN-106 with 1,6-dihydroxy-5-methoxy-2-(methoxymethyl)anthracene-9,10-dione molecules; and residues GLU-326, GLU-349, and ASN-345 residues with quercetin molecules. The shorter hydrogen bonding distances imply stronger binding affinities. Additionally, the more stable binding conformation was associated with the lower required binding energy. Binding energies of ≤ -4.25 kcal/mol, ≤ -5.0 kcal/mol, and ≤ -7.0 kcal/mol indicate weak, good, and strong binding activities, respectively. The molecular docking analysis in this study identified JunB, c-Jun, STAT3, and MAPK3/1 as target proteins due to their critical roles in the pathophysiology of POI. JunB and c-Jun could regulate autophagy, with their expression responding to autophagy-inducing signals. Autophagy is essential for maintaining mitochondrial health and removing damaged mitochondria, contributing to alleviating POI [33]. STAT3 is involved in autophagy through various pathways, exerting a protective effect on the ovaries tissue, including both oocytes and their surrounding cumulus cells within cumulus-oocyte complexes (COCs) [34]. The MAPK3/1 pathway is associated with growth hormone-mediated reduction of aneuploidy in aged oocytes, thereby improving the quality of denuded oocytes (DOs) following cumulus cell removal [35]. These target proteins were selected to better understand their mechanisms in POI and to explore

their potential as therapeutic targets at the molecular level. Overall, these data suggest that 1,6-dihydroxy-5-methoxy-2-(methoxymethyl)anthracene-9,10-dione molecules, formononetin and naringenin may be the key active components of HSYLF in the treatment of POI.

PPI network analysis showed that the hub genes of HSYLF in treating POI included heat shock protein 90 alpha family class A member 1, Jun, MAPK3, STAT3, and TP53. MAPK3, a member of the MAPK family, regulates a variety of cellular processes, including proliferation, differentiation, and cell cycle progression, in response to various extracellular signals. The activity of MAPK3 during oocyte maturation is crucial for granulosa cell function [36]. STAT3, a member of the STAT family, plays an essential role in processes such as cell proliferation, differentiation, and apoptosis. STAT3 has been reported to be capable of entering mitochondria, where it regulates the activity of electron transport chain complex enzymes, thereby affecting mitochondrial function [37]. Additionally, TP53 is closely related to ovarian granulosa cell apoptosis and proliferation [38]. GO and KEGG enrichment analyses indicated that the anti-POI targets of HSYLF mainly regulated response to xenobiotic stimulus, cellular response to chemical stress, and response to oxidative stress, with the main manifestation observed in responses to oxidative stress and response to ROS.

Highly correlated signaling pathways included the endocrine resistance, TNF signaling pathway, interleukin (IL)-17 signaling pathway, chemical carcinogenesis—receptor activation, and AGE-RAGE signaling pathway in diabetic complications. Therefore, HSYLF might play an important role in treating POI by regulating these signaling pathways.

TNF-α activates the Toll-like receptor 4 signaling pathway, further triggering the nuclear factor-κB (NF-κB) signaling pathway. Such a process promotes the phosphorylation and nuclear translocation of NF-κB, leading to an increased expression of pro-inflammatory factors, such as IL-6 and TNF-α in ovarian granulosa cells. During ovulation, TNF-α exhibits dual functions. On the one hand, TNF-α promotes the growth of preantral granulosa cells, inhibits differentiation, and enhances vascularization around the follicle, thus facilitating follicular rupture and ovulation. On the other hand, TNF-α can promote the apoptosis of luteinizing granulosa cells after ovulation, inhibit luteogenesis, and facilitate luteolysis. These results indicated that the mechanism of TNF-α is complex. Additionally, TNF-α can induce inflammatory responses, promote cell proliferation and survival, and trigger cell differentiation and apoptosis. The activation of TNF-α also triggers the phosphorylation and degradation of IκB proteins, releasing NF-κB (p65/p50 complex) for translocation to the nucleus. In the nucleus, NF-κB binds to specific DNA sequences, regulating the expression of genes associated with cell proliferation, survival, and apoptosis [39–41]. This regulatory mechanism may lead to increased proliferation of ovarian granulosa cells and potential induction of apoptosis, thereby significantly impacting ovarian physiological function.

IL-17 activates MAPK signaling pathways, including extracellular signal-regulated kinase, c-Jun N-terminal kinase, and p38 MAPK, which are crucial for cell proliferation, differentiation, and survival. By increasing the phosphorylation of proteins in the MAPK pathway, IL-17 promotes the growth of ovarian granulosa cells. Additionally, IL-17 can enhance the expression of pro-inflammatory factors, regulate the ovarian environment, and promote angiogenic factors such as vascular endothelial growth factor, increasing follicular vascularization and ensuring adequate nutrient and oxygen supply. Therefore, IL-17 facilitates the growth and vascularization of granulosa cells, influencing follicular development and ovarian function [42].

Oxidative and carbonyl stress can be mediated by the AGE-RAGE signaling pathway, and the accumulation of AGEs leads to accelerated ovarian aging [43]. AGEs binding to RAGE can initiate a cascade of intracellular signaling, activating various inflammatory pathways, including NF-κB. This activation promotes the expression of pro-inflammatory cytokines, resulting in a chronic inflammatory state in the ovarian microenvironment. Under the condition of ovarian aging, the accumulation of AGEs exacerbates oxidative stress, leading to mitochondrial dysfunction and elevated levels of ROS. Such results can cause cellular damage, including ovarian cell apoptosis, thereby reducing ovarian reserve and impacting overall reproductive function [44].

Additionally, AGEs accelerate the activation of primordial follicles through the AGE-RAGE pathway; however, premature activation can result in the early depletion of the primordial follicle pool. Moreover, AGEs can also promote the proliferation of ovarian granulosa cells and oocytes, accelerating the activation of primordial follicles in the ovary, which may further accelerate ovarian aging and lead to ROS [45].

HSYLF is speculated to significantly improve ovarian function in patients with POI, considering that mitochondria are the site of ROS production and the primary target of oxidative damage. It is inferred that HSYLF may improve hormone levels and oxidative stress response by modulating its fluorescence intensity, distribution, morphology, quantity, and activity levels.

Pan et al. discovered [46] that massive accumulations of free radicals and ROS can exert detrimental effects on cells, such as increased mitochondrial membrane permeability, destruction of cristae structure, and reduced

numbers of mitochondria debris. [47, 48], contributing to mitochondrial dysfunction [49]. Excessive ROS generation can destroy the ovarian follicular granulosa cells, luteinize follicles, and induce granulosa cell apoptosis [50]. When granulosa cells undergo apoptosis, oocytes lose the signals and energy required for physiological activities, resulting in halted development. This can lead to follicular atresia or even failure, further causing the decrease in ovarian reserve function. Moreover, this decrease severely impacts the dynamic characteristics of mitochondrial biogenesis of surrounding granulosa cells, forming a vicious cycle, and ultimately promoting the progress of POI [51–53].

Through the animal experiments, HSYLF might improve ovarian function in POI mice by decreasing mitochondrial ROS, increasing membrane potential, and improving mitochondrial function. These experimental results confirmed that the AMH levels in the model blank group of mice were significantly reduced, while the levels in the high-dose HSYLF group were markedly higher compared to the model blank group and approached those of the normal control group, indicating that HSYLF could improve ovarian function. Intragastric administration of HSYLF reduced ROS levels, with greater benefits observed in the TCM-treated group relative to the Western medicine group. Microscopy and fluorescence staining images of mitochondria revealed stronger fluorescence in the high-dose HSYLF group, with improved distribution, morphology, and quantity of mitochondria. According to the mitochondrial fluorescence staining images and electron microscopy, the number and morphology of mitochondria were significantly improved in the HSYLF treatment groups, indicating restored mitochondrial function. The membrane potential was notably increased, suggesting a significant effect of HSYLF on mitochondrial activity. The presence of HSYLF could modify hormone levels and oxidative stress responses in POI mice by altering fluorescence intensity, distribution, morphology, quantity, and activity level of mitochondria in oocytes, thereby improving oocyte quality and ovarian function.

In this study, we explored the methods for selecting disease targets using the DisGeNET and GeneCards databases and acknowledged the significant advantages of the Gene Expression Omnibus dataset in terms of accuracy for gene expression analysis. The DisGeNET and GeneCards databases were the initial choice due to their extensive coverage. However, in future research, the use of the Gene Expression Omnibus dataset will be prioritized to enhance data accuracy and improve the reliability of target selection. This study primarily focused on the mitochondrial regulatory effects of HSYLF on ovarian function, and thus expression validation for specific targets, such as STAT3, Jun, and TP53, was not conducted. Nevertheless, these targets might play critical roles in the pathogenesis of POI. Future research will involve more in-depth validation of these target expressions to reveal the potential multi-target regulatory mechanisms of HSYLF, providing a more comprehensive scientific basis for its mechanisms of action. Furthermore, based on the current animal experiment results, the potential of HSYLF in treating POI is recognized. However, animal experiment results may not fully reflect the physiological and pathological conditions in humans. Therefore, future research should include systematic clinical trials in a clinical setting to validate the safety and efficacy of HSYLF in humans. These trials will contribute comprehensively to assessing the therapeutic potential of HSYLF, further elucidating its regulatory effects on mitochondrial function and oxidative stress responses across multiple signaling pathways. This study provides definite evidence for the molecular mechanisms of HSYLF in treating POI by decreasing mitochondrial ROS, increasing membrane potential, and improving mitochondrial function. The treatment of POI with HSYLF may affect the cellular response to oxidative stress and ROS, thereby affecting the oocyte mitochondrial function and maintaining the normal function of ovarian granulosa cells. Findings on active components and related key targets of HSYLF also confirmed its characteristics of multi-component, multi-target, multi-pathway, and holistic regulatory effects against POI. The study establishes a theoretical basis for further research on the treatment of POI with HSYLF. These results need to be generalized with further mechanistic studies, and the deep clinical value of HSYLF should be investigated in the future.

Supplementary Information

The online version contains supplementary material available at https://doi.org/10.1186/s13048-024-01575-1.

Supplementary Material 1: Table S1. Medicines and reagents.

Supplementary Material 2: Table S2. Experimental setup and apparatus.

Supplementary Material 3: Table S3. Potential active components of HSYLF.

Supplementary Material 4: Table S4. PPI data.

Supplementary Material 5: Figure S1. PPI network of key targets (Lines representes their interaction, while the color indicates their degree value; the higher degree value is associated with the darker color, indicating closer to the core.)

Supplementary Material 6: Figure S2. Regulatory network diagram of key target function. (A). Key target-GO-BP; (B) Key target-GO-MF; (C) Key target-GO-CC.

Supplementary Material 7: Figure S3. Regulatory network diagram of key target-pathway.

Supplementary Material 8.

Acknowledgements
Not applicable.

Authors' contributions
Y.H.: Conception and design; Data analysis; Original draft preparation; Experimentation; Q.Z.: Review and editing; D.S.: Data curation; Experimentation; X.B.: Software; Experimentation.

Funding
This study is supported by Hangzhou Medical and Health Technology Project (No. 20220919Y043).

Data availability
The datasets used and/or analyzed during the current study are available from the corresponding author on reasonable request.

Declarations

Ethics approval and consent to participate
The animal study protocol was approved by the Animal Ethics Committee of Zhejiang Chinese Medical University for the handling of animals (protocol approval number: 20220639) and conducted in compliance with the institutional guidelines (Directive 2010/63/EU in Europe) for the care and use of animals.

Consent for publication
Not applicable.

Competing interests
The authors declare no competing interests.

Author details
[1]TCM Gynecology Department, Hangzhou Hospital of Traditional Chinese Medicine, NO.453 Ti Yuchang Road, Hangzhou 310007, Zhejiang, China. [2] Geriatric Department, Hangzhou Hospital of Traditional Chinese Medicine, NO.453 Ti Yuchang Road, Hangzhou 310007, Zhejiang, China.

Received: 19 September 2024 Accepted: 8 December 2024
Published online: 27 December 2024

References

1. Gowri V, Al Shukri M, Al-Farsi FA, Al-Busaidi NA, Dennison D, Al Kindi S, et al. Aetiological profile of women presenting with premature ovarian failure to a single tertiary care center in Oman. Post Reprod Health. 2015;21(2):63–8. https://doi.org/10.1177/2053369115587419.
2. Maciejewska-Jeske M, Szeliga A, Meczekalski B. Consequences of premature ovarian insufficiency on women's sexual health. Prz Menopauzalny. 2018;17(3):127–30. https://doi.org/10.5114/pm.2018.78557.
3. Lagergren K, Hammar M, Nedstrand E, Bladh M, Sydsjo G. The prevalence of primary ovarian insufficiency in Sweden; a national register study. BMC Womens Health. 2018;18 1:175. https://doi.org/10.1186/s12905-018-0665-2.
4. LIU, Jian, NIE, Guang-ning, YANG, Hong-yan. Hydrogen peroxide-induced oxidative stress model of human ovarian granulose cells. Guangdong Medical Journal. 2017;38 7:986–9; f9031c8cef70474584188c90a23ce419.
5. Jia-Lin HE, Xiao-Hong F, Tao G. studies on effects of yulin granule on uterine and ovarian er and hypothalamic arcuate nuclei ultrastructure in rats with ovulatory dysfunction. Chinese Journal of Traditional Medical Science Technology. 2008;86 2:90–2+79–80; 52270519640b8a318d88e8e7f3f12e46.
6. Jia-Lin HE, editor. Clinical Study on the Treatment of 50 Patients with Kidney Deficiency Type Ovarian Reserve Function Decline with Yulin Formula. 2011 Zhejiang Society of Traditional Chinese Medicine Gynecology Branch Academic Annual Meeting and Advanced Training Course on Integrated Traditional Chinese and Western Medicine Prevention and Treatment of Reproductive Disorders; 2011.
7. Hopkins AL. Network pharmacology. Nat Biotechnol. 2007;25(10):1110–1. https://doi.org/10.1038/nbt1007-1110.
8. Zhang R, Zhu X, Bai H, Ning K. Network pharmacology databases for traditional chinese medicine: review and assessment. Front Pharmacol. 2019;10:123. https://doi.org/10.3389/fphar.2019.00123.
9. Ru J, Li P, Wang J, Zhou W, Li B, Huang C, et al. TCMSP: a database of systems pharmacology for drug discovery from herbal medicines. J Cheminform. 2014;6:13. https://doi.org/10.1186/1758-2946-6-13.
10. Safran M, Chalifa-Caspi V, Shmueli O, Olender T, Lapidot M, Rosen N, et al. Human gene-centric databases at the weizmann institute of science: genecards, UDB, CroW 21 and HORDE. Nucleic Acids Res. 2003;31(1):142–6. https://doi.org/10.1093/nar/gkg050.
11. Szklarczyk D, Gable AL, Lyon D, Junge A, Wyder S, Huerta-Cepas J, et al. STRING v11: protein-protein association networks with increased coverage, supporting functional discovery in genome-wide experimental datasets. Nucleic Acids Res. 2019;47(D1):D607–13. https://doi.org/10.1093/nar/gky1131.
12. Shannon P, Markiel A, Ozier O, Baliga NS, Wang JT, Ramage D, et al. Cytoscape: a software environment for integrated models of biomolecular interaction networks. Genome Res. 2003;13(11):2498–504. https://doi.org/10.1101/gr.1239303.
13. Berman HM, Battistuz T, Bhat TN, Bluhm WF, Bourne PE, Burkhardt K, et al. The protein data bank. Acta Crystallogr D Biol Crystallogr. 2002;58 Pt 6 No 1:899–907. https://doi.org/10.1107/s0907444902003451.
14. Morris GM, Huey R, Lindstrom W, Sanner MF, Belew RK, Goodsell DS, et al. AutoDock4 and AutoDockTools4: automated docking with selective receptor flexibility. J Comput Chem. 2009;30(16):2785–91. https://doi.org/10.1002/jcc.21256.
15. Kim S, Chen J, Cheng T, Gindulyte A, He J, He S, et al. PubChem in 2021: new data content and improved web interfaces. Nucleic Acids Res. 2021;49(D1):D1388–95. https://doi.org/10.1093/nar/gkaa971.
16. Trott O, Olson AJ. AutoDock Vina: improving the speed and accuracy of docking with a new scoring function, efficient optimization, and multithreading. J Comput Chem. 2010;31(2):455–61. https://doi.org/10.1002/jcc.21334.
17. Seeliger D, de Groot BL. Ligand docking and binding site analysis with PyMOL and Autodock/Vina. J Comput Aided Mol Des. 2010;24(5):417–22. https://doi.org/10.1007/s10822-010-9352-6.
18. Feng X, Wang D, Hu L, Lu H, Ling B, Huang Y, et al. Dendrobium officinale polysaccharide ameliorates polycystic ovary syndrome via regulating butyrate dependent gut-brain-ovary axis mechanism. Front Endocrinol (Lausanne). 2022;13:962775. https://doi.org/10.3389/fendo.2022.962775.
19. Cora MC, Kooistra L, Travlos G. Vaginal cytology of the laboratory rat and mouse: review and criteria for the staging of the estrous cycle using stained vaginal smears. Toxicol Pathol. 2015;43(6):776–93. https://doi.org/10.1177/0192623315570339.
20. Meirow D, Lewis H, Nugent D, Epstein M. Subclinical depletion of primordial follicular reserve in mice treated with cyclophosphamide: clinical importance and proposed accurate investigative tool. Hum Reprod. 1999;14(7):1903–7. https://doi.org/10.1093/humrep/14.7.1903.
21. Juan Z, Yuexi Z, Bo D, Gang W, Zhaoping Y, Di X, et al. Establishment and evaluation of a rabbit model of premature ovarian failure induced by cyclophosphamide. Chinese J Comparative Med. 2018;28 1:6:6. https://doi.org/10.3969/j.issn.1671-7856.2018.01.007.
22. Golezar S, Ramezani Tehrani F, Khazaei S, Ebadi A, Keshavarz Z. The global prevalence of primary ovarian insufficiency and early menopause: a meta-analysis. Climacteric. 2019;22(4):403–11. https://doi.org/10.1080/13697137.2019.1574738.
23. Wang R, Zhao Y, Miao C, Chen Y, Ren N, Yang L, et al. Investigation of the mechanisms and experimental verification of yulin formula in the treatment of diminished ovarian reserve via network pharmacology. Drug Des Dev Ther. 2023;17:2147–63. https://doi.org/10.2147/dddt.S413142.
24. Yu J, Zhao P, Niu J, Wang J, Hao Q. Research on phytoestrogenic effect of formononetin. China J Chin Materia Med. 2010;35(22):3060–4. 47ee209f9f5ce5047c97132175661b5a.
25. El-Bakoush A, Olajide OA. Formononetin inhibits neuroinflammation and increases estrogen receptor beta (ERbeta) protein expression in BV2 microglia. Int Immunopharmacol. 2018;61:325–37. https://doi.org/10.1016/j.intimp.2018.06.016.
26. Sugimoto M, Ko R, Goshima H, Koike A, Shibano M, Fujimori K. Formononetin attenuates H(2)O(2)-induced cell death through decreasing ROS level by PI3K/Akt-Nrf2-activated antioxidant gene expression and suppressing MAPK-regulated apoptosis in neuronal SH-SY5Y cells. Neurotoxicology. 2021;85:186–200. https://doi.org/10.1016/j.neuro.2021.05.014.

27. Hernandez-Aquino E, Muriel P. Beneficial effects of naringenin in liver diseases: Molecular mechanisms. World J Gastroenterol. 2018;24(16):1679–707. https://doi.org/10.3748/wjg.v24.i16.1679.
28. Al-Rejaie SS, Aleisa AM, Abuohashish HM, Parmar MY, Ola MS, Al-Hosaini AA, et al. Naringenin neutralises oxidative stress and nerve growth factor discrepancy in experimental diabetic neuropathy. Neurol Res. 2015;37(10):924–33. https://doi.org/10.1179/1743132815Y.0000000079.
29. Wu LH, Lin C, Lin HY, Liu YS, Wu CY, Tsai CF, et al. Naringenin suppresses neuroinflammatory responses through inducing suppressor of cytokine signaling 3 expression. Mol Neurobiol. 2016;53(2):1080–91. https://doi.org/10.1007/s12035-014-9042-9.
30. Kapoor R, Rizvi F, Kakkar P. Naringenin prevents high glucose-induced mitochondria-mediated apoptosis involving AIF. Endo-G and caspases Apoptosis. 2013;18(1):9–27. https://doi.org/10.1007/s10495-012-0781-7.
31. Kocyigit A, Koyuncu I, Taskin A, Dikilitas M, Bahadori F, Turkkan B. Antigenotoxic and antioxidant potentials of newly derivatized compound naringenin-oxime relative to naringenin on human mononuclear cells. Drug Chem Toxicol. 2016;39(1):66–73. https://doi.org/10.3109/01480545.2015.1026973.
32. Kemp G, Rose P, Lurain J, Berman M, Manetta A, Roullet B, et al. Amifostine pretreatment for protection against cyclophosphamide-induced and cisplatin-induced toxicities: results of a randomized control trial in patients with advanced ovarian cancer. J Clin Oncol. 1996;14(7):2101–12. https://doi.org/10.1200/JCO.1996.14.7.2101.
33. Yogev O, Shaulian E. Jun proteins inhibit autophagy and induce cell death. Autophagy. 2010;6(4):566–7. https://doi.org/10.4161/auto.6.4.11950.
34. You L, Wang Z, Li H, Shou J, Jing Z, Xie J, et al. The role of STAT3 in autophagy. Autophagy. 2015;11(5):729–39. https://doi.org/10.1080/15548627.2015.1017192.
35. Luo YY, Zeng X, Zhu L, Li C, Xie J, Dong Q, et al. Growth hormone reduces aneuploidy and improves oocytes quality by JAK2-MAPK3/1 pathway in aged mice. J Transl Med. 2023;21 1:426. https://doi.org/10.1186/s12967-023-04296-z.
36. Gratao AA, Dahlhoff M, Sinowatz F, Wolf E, Schneider MR. Betacellulin overexpression in the mouse ovary leads to MAPK3/MAPK1 hyperactivation and reduces litter size by impairing fertilization. Biol Reprod. 2008;78(1):43–52. https://doi.org/10.1095/biolreprod.107.062588.
37. Tscherner A, Brown AC, Stalker L, Kao J, Dufort I, Sirard MA, et al. STAT3 signaling stimulates miR-21 expression in bovine cumulus cells during in vitro oocyte maturation. Sci Rep. 2018;8 1:11527. https://doi.org/10.1038/s41598-018-29874-w.
38. Sirotkin AV, Petrak J, Alwasel S, Harrath AH. Apoptosis signal-regulating kinase (ASK1) and transcription factor tumor suppressor protein TP53 suppress rabbit ovarian granulosa cell functions. Anim Reprod Sci. 2019;204:140–51. https://doi.org/10.1016/j.anireprosci.2019.03.018.
39. He F, Liu Y, Li T, Ma Q, Yongmei Z, He P, et al. MicroRNA-146 attenuates lipopolysaccharide induced ovarian dysfunction by inhibiting the TLR4/NF- κB signaling pathway. Bioengineered. 2022;13(5):11611–23. https://doi.org/10.1080/21655979.2022.2070584.
40. Zhang C, Yu D, Mei Y, Liu S, Shao H, Sun Q, et al. Single-cell RNA sequencing of peripheral blood reveals immune cell dysfunction in premature ovarian insufficiency. Front Endocrinol. 2023;14:1129657. https://doi.org/10.3389/fendo.2023.1129657.
41. Kunicki M, Rzewuska N, Gross-Kępińska K. Immunophenotypic profiles and inflammatory markers in premature ovarian insufficiency. J Reprod Immunol. 2024;164:104253. https://doi.org/10.1016/j.jri.2024.104253.
42. Hu F, Zhou X, Jiang Y, Huang X, Sheng S, Li D. Effect of myrcene on Th17/Treg balance and endocrine function in autoimmune premature ovarian insufficiency mice through the mapk signaling pathway. Protein Pept Lett. 2022;29(11):954–61. https://doi.org/10.2174/0929866529666220822100604.
43. Tatone C, Amicarelli F. The aging ovary–the poor granulosa cells. Fertil Steril. 2013;99(1):12–7. https://doi.org/10.1016/j.fertnstert.2012.11.029.
44. Park SU, Walsh L, Berkowitz KM. Mechanisms of ovarian aging. Reproduction (Cambridge, England). 2021;162(2):R19–r33. https://doi.org/10.1530/rep-21-0022.
45. Nan Z, Xiao-Yuan H, Jin-Jing LI, Hong-Shan GE. Effect of advanced glycation end products on ovarian primordial follicles. J Reprod Med. 2018;27 6:6. https://doi.org/10.3969/j.issn.1004-3845.2018.06.012.
46. Loren P, Sanchez R, Arias ME, Felmer R, Risopatron J, Cheuqueman C. Melatonin scavenger properties against oxidative and nitrosative stress: impact on gamete handling and in vitro embryo production in humans and other mammals. Int J Mol Sci. 2017;18; https://doi.org/10.3390/ijms18061119.
47. Pan YF, Wang YY, Chen JW, Fan YM. Mitochondrial metabolism's effect on epigenetic change and aging. Yi Chuan. 2019;41(10):893–904. https://doi.org/10.16288/j.yczz.19-065.
48. Feng D, Jia Y, Xiang-Yang LI, Qiong WU, Shao-Ying Z, Lan W. Cadmium induces apoptosis in PK-15 cells through oxidative stress and mitochondrial damage. chinese journal of biochemistry. Mol Biol. 2018;34 11:9. https://doi.org/10.13865/j.cnki.cjbmb.2018.11.08.
49. Lin CL, Lee CH, Chen CM, Cheng CW, Chen PN, Ying TH, et al. Protodioscin induces apoptosis through ROS-mediated endoplasmic reticulum stress via the jnk/p38 activation pathways in human cervical cancer cells. Cell Physiol Biochem. 2018;46(1):322–34. https://doi.org/10.1159/000488433.
50. Jian L, Guang-Ning N, Hong-Yan Y. Hydrogen peroxide-induced oxidative stress model of human ovarian granulose cells. Guangdong Med J. 2017;38(7):986–9.
51. Zhang J, Liu Y, Yao W, Li Q, Liu H, Pan Z. Initiation of follicular atresia: gene networks during early atresia in pig ovaries. Reproduction. 2018;156(1):23–33. https://doi.org/10.1530/REP-18-0058.
52. May-Panloup P, Boucret L, Chao de la Barca JM, Desquiret-Dumas V, Ferre-L'Hotellier V, Moriniere C, et al. Ovarian ageing: the role of mitochondria in oocytes and follicles. Hum Reprod Update. 2016;22:725–43. https://doi.org/10.1093/humupd/dmw028.
53. Dong-Na H, Wen-Juan R, Xiao-Qin F, Xin L, Zhi-Ping W, Jian-Rong L, et al. Study on the role of granulosa cell complex for in vitro maturation of oocytes. J Reprod Med. 2019;28(3):279–83. https://doi.org/10.3969/j.issn.1004-3845.2019.03.013.

Publisher's Note